NJC

PAPER

View Article Online
View Journal

Cite this: DOI: 10.1039/c5nj00837a

Morphology-controlled self-assembly of an amphiphilic perylenetetracarboxylic diimide dimer-based semiconductor: from flower clusters to hollow spheres†

Liuqun Xu,[a] Dameng Gao,[a] Jingang Song,[b] Li Shen,[c] Wenmiao Chen,[b] Yanli Chen*[ac] and Shuxiang Zhang*[a]

Received (in Montpellier, France) 5th April 2015,
Accepted 13th May 2015

DOI: 10.1039/c5nj00837a

www.rsc.org/njc

A novel amphiphilic heptafluorobutyl-substituted perylenetetracarboxylic diimide dimer, 1-amino-3,5-[*N*-amino-*N*′-heptafluorobutyl-1,6,7,12-tetra(*tert*-butylphenoxy)-3,4:9,10-perylene diimide]-2,4,6-triazine, has been synthesized. The self-assembly properties of this dimer in mixed tetrahydrofuran/water (THF–H_2O) solvents of different volume ratios were studied. Fine-tuning of the non-covalent interactions of the amphiphilic molecules in 75/25, 50/50 and 25/75 THF/H_2O v/v mixtures led to the formation of micro-flower clusters, micro-bowknots and nano-hollow spheres, respectively. The conductivity of the micro-bowknots was about one order of magnitude higher than the conductivity of the micro-flower clusters and the nano-hollow spheres. On saturation with hydrazine vapour, the conductivity was dramatically increased by about three, four and five orders of magnitude for the micro-bowknots, micro-flower clusters and nano-hollow spheres, respectively, compared with the aggregates in air. These results suggest new opportunities for the design and preparation of high-performance sensing devices using a combination of molecular design and controlled intermolecular interactions in mixed solvents.

1. Introduction

Perylenetetracarboxylic diimides (PDIs) are valuable functional dyes with promising applications in many areas of scientific research.[1] The unique optical and electronic characteristics of PDIs, such as their strong photoelectrochemical activity and semiconducting properties, have attracted much attention for applications in electronic and optoelectronic devices,[2,3] chemical sensors[4] and catalysis.[5] For most of these applications, the properties of the molecular devices are closely related to the microstructures and morphologies of the molecular materials. Therefore the development and study of highly ordered supramolecular structures are not only of primary importance in gaining a better understanding of the structure–property relationships of these dyes, but are also critical steps towards the application of PDIs in nanoscale electronic and optoelectronic devices. Great progress has been achieved in the past decade towards the construction of ordered supramolecular self-assemblies from specifically engineered PDI molecules *via* the introduction of different functional groups onto either the imide nitrogen or the bay positions of the PDI ring.[6–8] Depending on various non-covalent interactions, including π–π stacking, hydrogen bonding, electrostatic interactions, metal ion coordination and side-chain hydrophobic interactions, the self-assembly of functionalized PDI dyes has yielded a variety of nanostructures, such as nanowires, nanoribbons, nanorods, nanotubes, hollow vesicles and nanoparticles.[9–16] However, the self-assembly of functional molecules into a prerequisite nanostructure with desirable dimensions and morphology *via* the control and optimization of the intermolecular interactions remains a great challenge.[17,18] Studies have shown that the self-assembly process for PDI molecules is dominated not only by the molecular structure, but also by a balance of intermolecular interactions between the PDI molecules and between the PDI and solvent molecules. Except for the intrinsic effects from the molecular structure, the self-assembly of PDIs depends largely on the polarity of the solvent. For example, we have observed that a symmetrical amphiphilic PDI derivative with hydroxyethyl substituents linked at the imide positions of the perylene ring

[a] *Shandong Provincial Key Laboratory of Fluorine Chemistry and Chemical Materials, School of Chemistry and Chemical Engineering, University of Jinan, Jinan 250022, China. E-mail: chm_chenyl@ujn.edu.cn*
[b] *Department of Chemistry, Shandong University, Jinan 250100, China*
[c] *School of Science, China University of Petroleum, Qingdao 266580, China. E-mail: yanlichen@upc.ed.cn*

† Electronic supplementary information (ESI) available: Peak positions of absorption for **2PDIF-TAZ** in THF and the self-assembled **2PDIF-TAZ** micro-flower clusters, micro-bowknots, and nano-hollow spheres dispersed in water. The energy-minimized molecular structure of **2PDIF-TAZ**. The differential pulse voltammetry (DPV) curves and experimental data of **2PDIF-TAZ**. See DOI: 10.1039/c5nj00837a

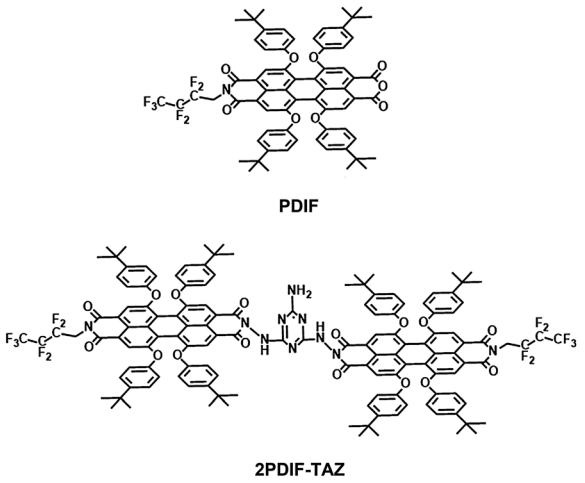

Scheme 1 Molecular structures of PDIF and **2PDIF-TAZ**.

formed nanobelt dendrites in methanol and nanosheets in *n*-hexane.[18] Xu *et al.*[19] reported a 1,7-bis-pyridinoyl perylene diimide amphiphile that self-assembled into hollow nanospheres in methanol and micro-rose flowers in ethanol. Yang *et al.*[20] found that the self-assembly of an asymmetrical PDI amphiphile with two different hydrophobic and hydrophilic side-chains yielded nanofibres in polar solvents and nanostrips in non-polar solvents. The combination of hydrogen bonding with solution-based self-assembly techniques is a rational design strategy to achieve PDI aggregates with highly ordered structures. With this in mind, we report here the synthesis and self-assembly of an amphiphilic PDI dimer, 1-amino-3,5-[*N*-amino-*N*′-heptafluorobutyl-1,6,7,12-tetra(*tert*-butylphenoxy)-3,4:9,10-perylene diimide]-2,4,6-triazine (**2PDIF-TAZ**) (Scheme 1). The controlled self-assembly of **2PDIF-TAZ** molecules in tetrahydrofuran (THF)/H_2O mixed solvents with different volume ratios of 75/25, 50/50 and 25/75 results in microstructures with different morphologies, from flower clusters and bowknots to hollow spheres. This study provides a detailed and fundamental understanding of the factors that control the formation of self-assembled microstructures of conjugated amphiphiles.

2. Results and discussion

2.1 Molecular design and synthesis

Amphiphilic **2PDIF-TAZ** was designed with the idea of obtaining a PDI-based dimeric molecular structure with an intrinsic curvature, which is expected to make it possible to fabricate microstructures with tunable dimensions and morphologies.[21–23] In a dimeric **2PDIF-TAZ** molecule, each of the two PDI units consists of four *tert*-butylphenoxy groups at the bay positions and a hydrophobic perfluorinated alkane chain at one of its two imide nitrogen atoms. This ensures good solubility in common organic solvents and, in turn, good ability to be processed in solution. The linkage, a hydrophilic melamine ring, used to connect the two monomeric PDI units to form a PDI dimer provides the possibility of ordering the molecules in the self-assembly processes through intermolecular hydrogen bonding, as observed in PDI amphiphiles,[24,25] and other types of amphiphiles.[26] Amphiphilic **2PDIF-TAZ** was prepared following a previously reported procedure[24,25] and was characterized by a series of spectroscopic methods, including MALDI-TOF mass spectrometry and ^{1}H-NMR spectrometry.

2.2 Morphology of the aggregates

The morphologies of the aggregates formed in the THF/H_2O mixed solvents (75/25, 50/50 and 25/75 v/v) were examined by scanning electron microscopy (SEM). As shown in Fig. 1a, in 75/25 v/v THF/H_2O, **2PDIF-TAZ** assembles into a flower cluster morphology, about 10 μm long and 4 μm in width, organized by densely packed one-dimensional nanorods with an average length and width of about 3 μm and 300 nm, respectively. With an increase in the water content in the THF/H_2O mixed solvents from 75/25 to 50/50 v/v, remarkable morphologies varying from flower clusters to bowknots were obtained (Fig. 1b). The bowknot-like microstructures consisted of densely packed two-dimensional micro-sheets with an average length and width of about 3.6 μm and 1.3 μm. More interestingly, a further increase in the water content in the THF–H_2O mixed solvents led to a further change in the morphology of the self-assembled nanoscale aggregates. As shown in Fig. 1c, the **2PDIF-TAZ** molecules in 25/75 v/v THF/H_2O self-assembled into hollow spherical nanostructures with a diameter of 200–600 nm. The hollow feature of the nanospheres was further confirmed by TEM observation (Fig. 1d). Considering the large difference in the dielectronic constant between the protic H_2O (78.5) and aprotic THF (7.6), the strong dipole–dipole interactions between the dimeric **2PDIF-TAZ** and H_2O molecules were expected to facilitate the formation of the additional curvature and then the hollow nanospheres.[22] Nevertheless, the additional curvature can collapse when the H_2O content decreases to <50 vol% as a result of the reduced dipole–dipole interactions between the **2PDIF-TAZ** and the H_2O molecules. This was further supported by the fact that **2PDIF-TAZ** self-assembled into flower clusters and bowknot-like microstructures in the 75/25, 50/50 v/v THF/H_2O systems, rather than the hollow nanospheres as formed in the 25/75 v/v THF/H_2O system. This suggests that the water content in the mixed solvent systems has a large impact on the variation in the aggregated microstructures (morphologies) of amphiphilic **2PDIF-TAZ**. The dimension- and morphology-adjustable microstructures are highly desirable in practical applications.

2.3 Electronic absorption and fluorescence emission spectra of the aggregates

Fig. 2a shows the normalized absorption spectra of the **2PDIF-TAZ** in THF solution and its self-assembled aggregates formed in THF/H_2O mixed solvents from 75/25, 50/50 to 25/75 v/v; the corresponding experimental data are given in Table S1 (ESI†). As shown in Fig. 2a, **2PDIF-TAZ** in THF solution displays well-defined absorptions at about 573 and 533 nm, which can be attributed to the 0–0 and 0–1 vibronic band of the S_0–S_1 transition, respectively, whereas the observed absorption band

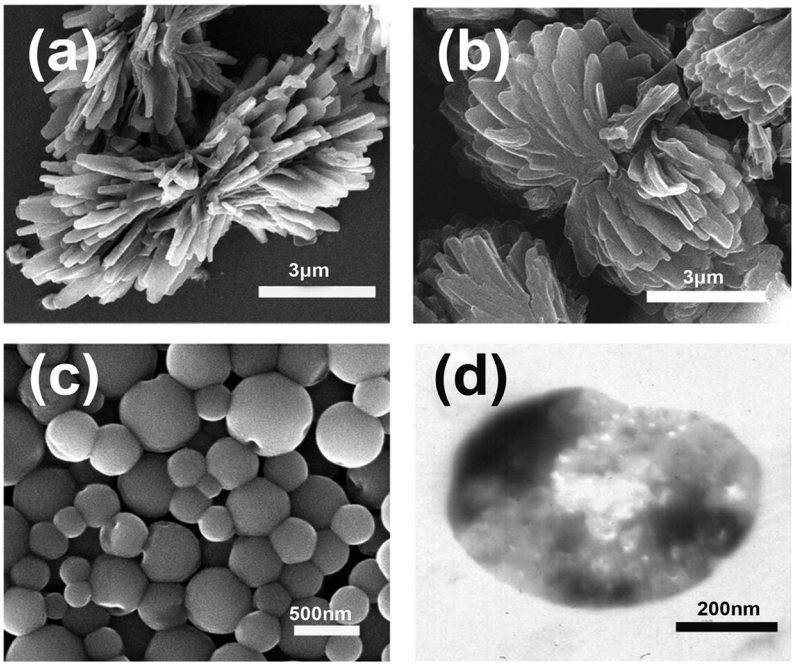

Fig. 1 SEM images of **2PDIF-TAZ** aggregates formed in THF/H_2O mixed solvents with volume ratios of (a) 75/25, (b) 50/50 and (c) 25/75 v/v. (d) A nanoscale hollow sphere formed in THF/H_2O (25/75 v/v) observed by TEM.

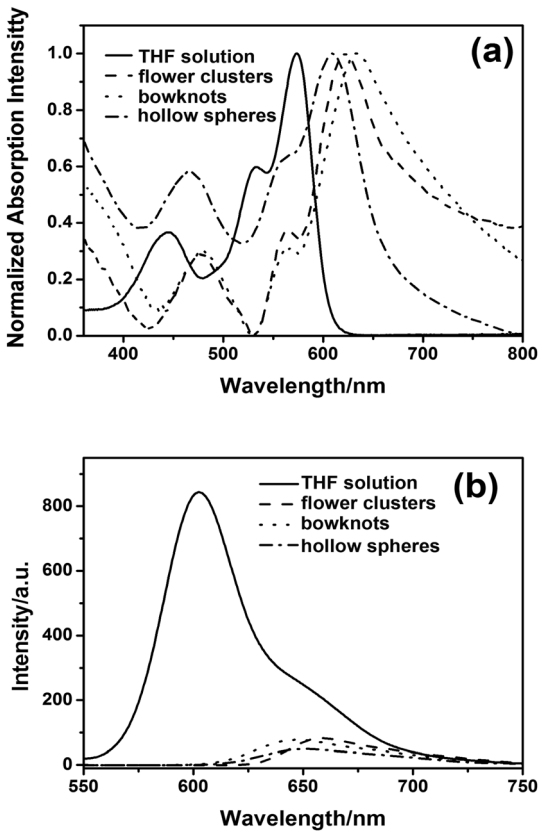

Fig. 2 (a) Normalized electronic absorption and (b) fluorescence emission spectra of **2PDIF-TAZ** in THF solution (solid line) and the self-assembled **2PDIF-TAZ** micro-flower clusters (dashed line), micro-bowknots (dotted line) and nano-hollow spheres (dash-dot line) dispersed in water. The excitation wavelength was 520 nm.

around 445 nm is attributed to the electronic S_0–S_2 transition. These are in good agreement with the peak positions observed for the monomer PDI derivatives with four phenoxy substituents at the bay area (1,6,7,12 positions of the perylene core).[27–29] The emission spectrum in THF solution (1×10^{-6} mol L^{-1}) with a band maximum at 602 nm is the mirror image of the absorption band and copies the characteristics of the PDI monomer's fluorescence spectrum (Fig. 2b). This result suggests that the two PDI units in the dimer **2PDIF-TAZ** do not interact in dilute solutions.[30] In contrast with their behaviour in THF solution, when dispersed in the THF/H_2O mixed solvents with volume ratios of 75/25, 50/50 and 25/75 v/v, the **2PDIF-TAZ** molecules aggregated as a result of significant intermolecular interactions, resulting in a distinct change in the electronic absorption spectrum (Fig. 2a). On aggregation, the absorption spectra of the self-assembled microstructures in the 75/25, 50/50 and 25/75 THF/H_2O v/v systems all have a significant red shift of the absorption maximum compared with that of **2PDIF-TAZ** in THF solution, which clearly indicates the formation of the J-type (edge-to-edge) aggregate.[20] Interestingly, together with the increasing content of water, the degree of the red shift increases from 48 nm for the flower clusters to 61 nm for the bowknots and then decreases to 34 nm for the hollow spheres.

These observations indicate that the water interacted with the **2PDIF-TAZ** molecules.[31] This suggests that the intermolecular interactions can be fine-tuned to produce varied microstructures by simply selecting the solvent to control the self-assembly process. Significant changes were also observed in the fluorescence spectra for **2PDIF-TAZ** on aggregation (Fig. 2b). More significantly, the fluorescence spectra displayed broad emission bands of relatively weak intensity in the range

648–659 nm with bathochromic shifts of 46–57 nm for the self-assembled microstructures. These spectral features are similar to those observed previously for aggregates of PDI-based dyes[30] and can be related to a pronounced structural and energetic relaxation process of the excited aggregates of dimeric **2PDIF-TAZ**.[29]

2.4 X-ray diffraction characterization of the aggregates

The internal structures of the three kinds of aggregates were investigated by XRD analysis (Fig. 3). The XRD measurements of the flower clusters showed that the short axis of the unit cell was 1.62 nm (Fig. 3a),[32] which is about 10% shorter than the total width of a dimeric **2PDIF-TAZ** molecule (along the transverse direction of the perylene rings) of 1.8 nm, which was obtained from the energy-optimized conformation of the molecule using the Gaussian 09 program at the AM1 semi-empirical level (Fig. S1, ESI†).

This is probably due to the strong hydrophobic interaction between the side-groups (*tert*-butylphenoxy groups), which usually results in side-group interdigitation and leads to a shortened length along the transverse direction of the perylene ring. It is worth noting that, in the wide-angle region, a well-defined diffraction at 0.30 nm should be attributed to the (triazine) N–H···N (triazine) hydrogen bond between the two neighbouring **2PDIF-TAZ** molecules,[33] leading to an edge-to-edge arrangement between the adjacent perylene chromophores of the **2PDIF-TAZ** molecules; a unit cell consisting of two **2PDIF-TAZ** molecules was therefore seen (Fig. 3a). In other words, during the molecular self-assembly process of this compound, a dimeric supramolecular structure was formed first through an intermolecular hydrogen bond between two **2PDIF-TAZ** molecules; this then acted as a building block and further self-assembled into the target micro-flower clusters depending mainly on the hydrophobic interactions between the *tert*-butylphenoxy groups of the **2PDIF-TAZ** molecules. This is also true for the bowknots formed in the 50/50 v/v THF/H_2O systems (Fig. 3b). A smaller lattice parameter (1.44 nm) was obtained for the short axis of the unit cell for the micro-bowknots, in line with a shortened distance of the (triazine) N–H···N (triazine) hydrogen bond (0.28 nm) between the two neighbouring **2PDIF-TAZ** molecules, implying stronger intermolecular interactions between the self-assembled microstructures formed in 50/50 v/v THF/H_2O than in 75/25 v/v THF/H_2O systems. This agrees with the conclusion from the electronic absorption spectroscopic properties. With an increasing proportion of water in the THF–H_2O mixtures, **2PDIF-TAZ** has a lower solubility and this facilitates molecular aggregation. The stronger hydrogen bonding interaction between the triazine groups may enhance the interdigitation between the side-groups of **2PDIF-TAZ**, leading to micro-sheet assembly and thus the formation of the bowknot-like microstructures. In addition, a relatively wide diffraction peak at 0.39 nm for the bowknots corresponds to the π–π stacking distance between the perylene–perylene rings of adjacent **2PDIF-TAZ** molecules (inset, Fig. 3b).[34] Unexpectedly, on increasing the content of water further to 75 vol%, the lattice parameter in the (001) direction increased from 1.44 nm for the bowknots to 1.56 nm for the nano-hollow spheres (Fig. 3c), suggesting that the intermolecular interaction between the **2PDIF-TAZ** molecules gradually decreases in this direction. The (triazine) N–H···N (triazine) hydrogen bonding interaction between the **2PDIF-TAZ** molecules is absent as a result of the dramatic decrease in solubility that led to rapid aggregation of the molecules with a lack of direction. As a consequence, solvent-tunable microstructures with controlled morphologies of **2PDIF-TAZ** were achieved depending on the competition and cooperation of various non-covalent interactions, including van der Waals, hydrogen bonding and hydrophilic–hydrophobic interactions, during the self-assembly process.

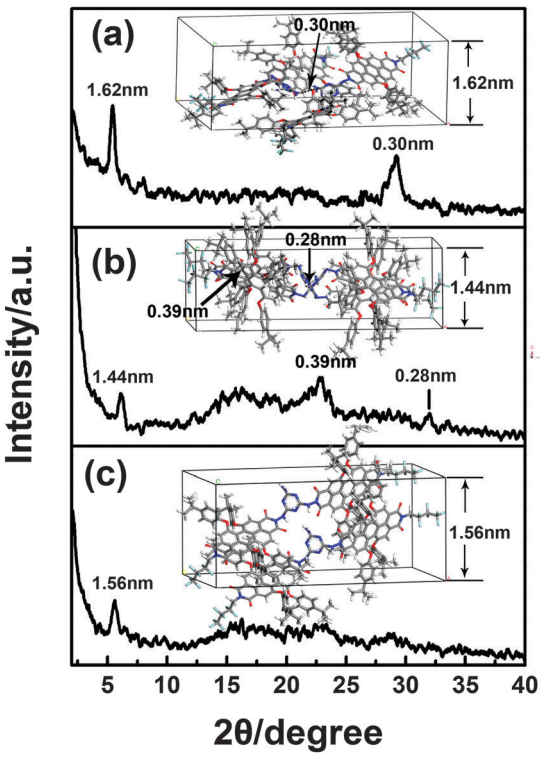

Fig. 3 XRD patterns of (a) micro-flower clusters, (b) micro-bowknots and (c) nano-hollow spheres.

2.5 Mechanism of formation of the aggregates

The different solubility of the amphiphilic **2PDIF-TAZ** or its hydrophilic and hydrophobic units in THF–H_2O mixed solvents offers a precise control of the dimensions and morphologies of the aggregate structures. On the basis of the experimental results, a formation mechanism for the supramolecular aggregates in THF–H_2O mixed solvent systems (with changing volume ratios) was proposed (Fig. 4). In 75/25 v/v THF/H_2O, the strong hydrophobic interaction between the side-groups (*tert*-butylphenoxy groups) of the **2PDIF-TAZ** molecules was expected to strengthen the intermolecular N–H···N hydrogen bonding interaction and thus resulted in the formation of one-dimensional nanorods. The original rods then tightly packed together, driven by the side-chains stacked between the perfluorinated alkane moieties, to form flower clusters (Fig. 4a). The bowknots were formed by a very similar process, but their

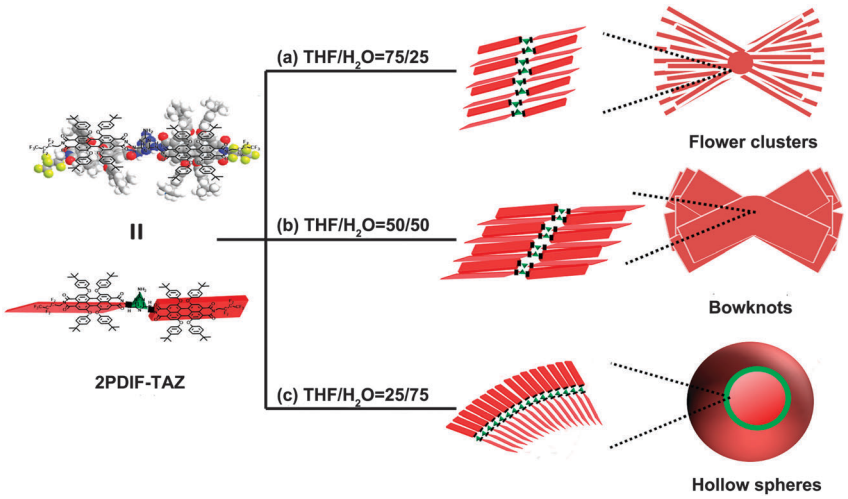

Fig. 4 Schematic illustration of the formation process of micro-flower clusters, micro-bowknots and nano-hollow spheres.

preliminary nanorods aligned and packed side-by-side, thereby forming planar bowknots depending on increased intermolecular interactions by virtue of both the side-groups stacked between the **PDIF** building blocks and hydrogen bonding between the melamine units of the **2PDIF-TAZ** molecules (Fig. 4b). In contrast with the intermolecular N–H···N hydrogen bonding formed in 75/25 and 50/50 v/v THF/H_2O mixed solvents, an increasing content of water up to 75 vol% weakened the intermolecular N–H···N hydrogen bonding, which limited the continuous growth of the flat-elongated rods. Water is a poor solvent for **2PDIF-TAZ**, but could bond with the melamine units of the **2PDIF-TAZ**,[31] whereas THF is a good solvent for **2PDIF-TAZ**. Therefore, in the 25/75 v/v THF/H_2O mixed solvent, the water bonded with the melamine units. The combination of strong hydrophobic interactions between the side-groups (*tert*-butylphenoxy groups) and the side-chains stacked between the perfluorinated alkane moieties among the **2PDIF-TAZ** molecules led to the formation of spherical nanostructures.[21] The resulting nanostructures can form many small holes (Fig. 1d) during the slow evaporation of the encapsulated water. During evaporation, the volume of the encapsulated water decreased, leading to the loosely packed **2PDIF-TAZ** rearranging into a dense packing structure and an interdigitated layer with low surface free energy. The nano-hollow spheres were then formed (Fig. 4c).

2.6 Current–voltage characteristics of the aggregates in air and saturated hydrazine vapour

The uniform aggregates of **2PDIF-TAZ** with well-defined microstructures are promising candidates for applications in electronic devices. To study the potentials of the three aggregates, diluted suspensions of molecular aggregates of **2PDIF-TAZ** formed in the mixed solvents were carefully dropped onto glass substrates of ITO interdigitated electrode (IDE) arrays. After complete evaporation of the solvents, the densely packed nanostructured films remained and adhered tightly to the ITO IDEs/glass substrate, allowing electron conductivity measurements to be made *in situ*. Fig. 5 shows the current–voltage (*I–V*) characteristics of the micro-flower clusters, micro-bowknots and nano-hollow spheres of **2PDIF-TAZ** in air and in saturated hydrazine vapour. According to the previously reported equation,[32,35] the electronic conductivities of

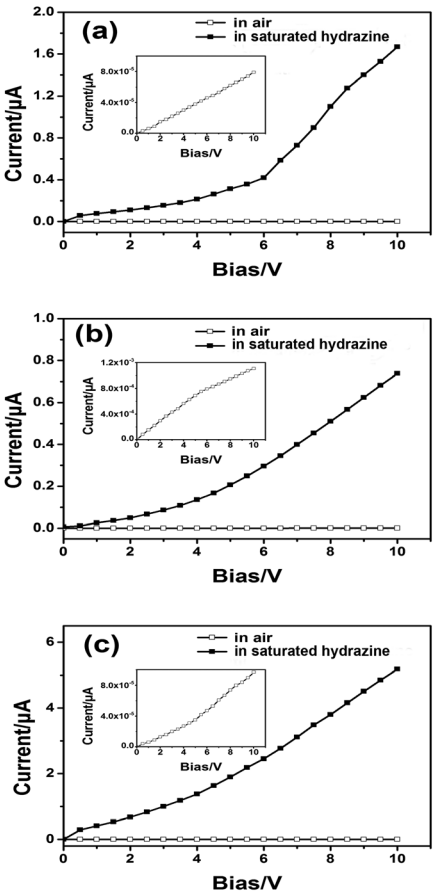

Fig. 5 *I–V* curves measured on **2PDIF-TAZ** (a) micro-flower clusters, (b) micro-bowknots and (c) nano-hollow spheres in air and in saturated hydrazine for 20 min. Inset, *I–V* curve in air from 0 to 10 V.

the three kinds of aggregates in air were calculated to be around 2.64×10^{-9} (micro-flower clusters), 3.82×10^{-8} (micro-bowknots) and 2.52×10^{-9} S cm^{-1} (nano-hollow spheres), respectively. Thus there is a significant dependence of the intermolecular interaction for **2PDIF-TAZ** aggregates: the higher the intermolecular interaction, the higher the mobility of the charge carriers, resulting in a higher current passing through the devices. In particular, compared with the other two aggregates, the conductivity of the micro-bowknots was significantly improved, which can be attributed to both the readily available π-stacks with adjacent planar molecules and stronger hydrogen bonding as well as side-group interdigitation interactions.[18]

Chemical doping is often used to tune the charge-carrier transport of a conducting organic semiconductor.[36] Therefore the change in conductivity of the resulting supramolecular aggregates was examined in saturated hydrazine vapour (Fig. 5). Hydrazine is a strong reductive reagent that is capable of giving an electron to the microstructures through a ground-state redox reaction (hydrazine, E^{o}_{ox} = +0.43 V *vs.* SCE;[37] **2PDIF-TAZ**, E^{o}_{red} = −0.63 V *vs.* SCE; Fig. S2 and Table S2, ESI†). Under an applied bias, the doped electrons rapidly migrated and led to a significant enhancement in the current (Fig. 5).

The conductivity of the hydrazine-doped micro-flower clusters, micro-bowknots and nano-hollow spheres extracted from the quasi-linear region at low bias (up to 5 V) was estimated at around 1.46×10^{-5}, 1.16×10^{-5} and 1.04×10^{-4} S cm^{-1}, respectively. Consequently, an approximately five orders of magnitude increase in conductivity was observed for the nano-hollow spheres on exposure to the saturated hydrazine vapour compared with their conductivity in air. However, only a three to four orders of magnitude increase was obtained for the micro-bowknots and micro-flower clusters. Moreover, compared with the PDI-based one-dimensional nanobelts reported in a previous study (three orders of magnitude increase in conductivity on saturation with hydrazine vapour),[37] the nano-hollow spheres in this study also showed a better performance in their sensitivity for the saturated vapour of hydrazine. These results indicate that the nano-hollow spherical structure is of significant advantage for increasing the sensitivity in gas sensors, probably as a result of a relatively large specific surface area that can provide more surface adsorption sites to interact with the gas. The present aggregate structures with such a high modulation of conductivity could be useful in a wide range of electronic and sensor devices. Efforts to explore these opportunities are already underway.

3. Conclusions

An amphiphilic PDI dimer has been synthesized. Micro-flower clusters, micro-bowknots and nano-hollow spheres were prepared in THF–H_2O solvent mixtures at various volume ratios. Micro-flower clusters, micro-bowknots and nano-hollow spheres showed semiconductor features, suggesting promising potential in electronic device applications. A highly sensitive hydrazine-sensing response was also observed in these microstructures. This study not only provides a pathway to tuning the structures and morphologies of PDI molecules, but also provides the possibility of constructing high-performance devices utilizing easily accessible control mechanisms. This will be valuable in designing and preparing PDI-based electronic devices with good performances.

4. Experimental

4.1 General

1*H*,1*H*-Heptafluorobutylamine was purchased from Aldrich. The dichloromethane for the electrochemical measurements was freshly distilled from CaH_2 under an atmosphere of nitrogen. Column chromatography was carried out on silica gel (200–300 mesh) with the indicated eluents. All other reagents and solvents were used as received. 1-Amino-3,5-dihyrazine-2,4,6-triazine and 1,6,7,12-tetra(4-*tert*-butylphenoxy)-perylene-3,4,9,10-tetracarboxylic dianhydride were prepared according to previously published procedures.[24,38]

4.2 Measurements

^{1}H-NMR spectra were recorded on a Bruker DPX 400 spectrometer in $CDCl_3$. The spectra were referenced internally with residual $CDCl_3$ (δ = 7.26 ppm). MALDI-TOF mass spectra were recorded on a Bruker BIFLEX III ultra-high-resolution Fourier-transform ion cyclotron resonance (FT-ICR) mass spectrometer with alpha-cyano-4-hydroxycinnamic acid as the matrix. Electrochemical measurements were carried out with a CHI760D voltammetric analyser. The cell consisted of inlets for a glassy carbon disc working electrode 3.0 mm in diameter and a silver wire counter electrode. The reference electrode was Ag/Ag$^+$ (0.01 mol dm^{-3}) and was connected to the solution *via* a Luggin capillary, the tip of which was placed close to the working electrode. The electrode was corrected for junction potentials by internal reference to the ferrocenium/ferrocene (Fc^+/Fc) couple [$E_{1/2}$(Fc^+/Fc) = 0.50 V *vs.* SCE]. Typically, a 0.1 mol dm^{-3} solution of [Bu_4N][ClO_4] in CH_2Cl_2 containing 0.5 mmol dm^{-3} of sample was purged with nitrogen for 15 min, then the differential pulse voltammogram was recorded at ambient temperature. The scan rate was 10 mV s^{-1}. The electronic absorption and fluorescence spectra were recorded on a UV-2550 spectrophotometer and an Edinburgh Instruments FLS920 spectrofluorimeter, respectively. The XRD experiments were carried out on a Bruker D8 FOCUS X-ray diffractometer. SEM images were obtained using a JEOL JSM-6700F field-emission scanning electron microscope. For the SEM imaging, Au (1–2 nm) was sputtered onto the grids to prevent charging effects and to improve the clarity of the image. The TEM images were obtained using a JEOL JEM-100CX II instrument. The substrates used in this study were successively cleaned with pure water, alcohol and dichloromethane.

4.3 Materials

4.3.1 Preparation of *N*-heptafluorobutylamine-1,6,7,12-tetra-(4-*tert*-butylphenoxy) perylene-3,4:9,10-tetracarboxylic-3,4-anhydride-9,10-imide (PDIF). A mixture of 1,6,7,12-tetra(4-*tert*-butylphenoxy)-perylene-3,4,9,10-tetracarboxylic dianhydride (0.2432 g, 0.025 mmol),

1*H*,1*H*-heptafluorobutylamine (34 μL, 0.024 mmol) and imidazole (1.324 g) in toluene (10 mL) was heated to reflux under nitrogen at 116 °C for 2 h. After cooling briefly, the volatiles were removed under reduced pressure. The solid was dissolved with a small amount of methylene chloride and was extracted with an excess of water to remove the imidazole. The product was dried and separated from the residue by column chromatography on silica gel with chloroform–hexane as the eluent. The compound was obtained as a red powder (43 mg, 15%). MALDI-TOF MS (*m*/*z*): calculated for $C_{68}H_{58}F_7NO_9$ 1166.2; found *m*/*z* $[MH]^+$ 1167.2. ^{1}H-NMR (400 MHz, $CDCl_3$): δ 8.29 (s, 4H, perylene), 7.25–7.27 (d, 8H, phenyl), 6.81–6.86 (d, 8H, phenyl), 4.15 (s, 2H, NCH_2), 1.31 (s, 36H, $C(CH_3)_3$).

4.3.2 Preparation of 1-amino-3,5-[*N*-amino-*N*′-heptafluorobutyl-1,6,7,12-tetra(*tert*-butylphenoxy)-3,4:9,10-perylene diimide]-2,4,6-triazine (2PDIF-TAZ). A mixture of **PDIF** (96.4 mg, 0.083 mmol), 1-amino-3,5-dihyrazine-2,4,6-triazine (6.2 mg, 0.039 mmol) in pyridine (2 mL) was purged with dry nitrogen for 15 min and then heated to reflux with stirring at 116 °C. After refluxing continuously for another 2 h, the reaction was stopped and the pyridine was removed under reduced pressure. The product was dried and separated from the residue by column chromatography on silica gel with chloroform–methanol as the eluent. The target compound was obtained as a purple powder (13 mg, 14%). MALDI-TOF MS (*m*/*z*): calculated for $C_{139}H_{120}F_{14}N_{10}O_{16}$ 2452.5; found *m*/*z* $[MH]^+$ 2453.6; ^{1}H-NMR (400 MHz, $CDCl_3$): δ 8.24 (s, 8H, perylene), 7.22–7.24 (d, 16H, phenyl), 6.80–6.83 (d, 16H, phenyl), 4.92 (s, 4H, NCH_2), 2.21 (s, 2H, NH), 2.06 (s, 2H, NH_2), 1.28 (s, 72H, $C(CH_3)_3$).

4.4 Procedures

The nanostructures of **2PDIF-TAZ** were fabricated by a previously reported phase transfer method.[14] In a typical preparation the solution of **2PDIF-TAZ** in THF was injected into ultrapure water with different THF/H_2O volume ratios of 75/25, 50/50 to 25/75, in which it was only poorly soluble. Subsequently, the self-assembly system was sealed with parafilm to avoid the evaporation of the THF–H_2O solvents, and to maintain the total volume constant. After being kept under ambient conditions without disturbance for 5 days, precipitates were separated from the solvents and transferred to the carbon-coated grid or SiO_2/Si surface for the SEM, TEM observations, and XRD measurement.

4.5 Device fabrication

The IDE array was composed of ten pairs of ITO electrode digits (fingers) deposited on a glass substrate with the following dimensions: 125 μm electrode width, 75 μm spacing, 5850 μm overlapping length and 20 nm electrode thickness. The suspension of molecular aggregates was carefully dropped onto the glass substrates with ITO IDEs. After complete evaporation of the solvents, the densely packed aggregates remained and adhered tightly to the IDEs/glass substrate (the process was repeated so that the channels of the IDEs were completely covered by the aggregates), allowing the electron conductivity measurements to be carried out *in situ*. The conductivity, σ, can be calculated according to the previously reported equation.[32,35]

The current–voltage characteristics were obtained with a Hewlett-Packard 4140B semiconductor characterization system at room temperature in air.

Acknowledgements

This work was financially supported by the National Natural Science Foundation of China (No. 21371073).

Notes and references

1 D. Gorl, X. Zhang and F. Würthner, *Angew. Chem., Int. Ed.*, 2012, **51**, 6328.
2 J. Mei, Y. Diao, A. L. Appleton, L. Fang and Z. Bao, *J. Am. Chem. Soc.*, 2013, **135**, 6724.
3 Y. Che, X. Yang, G. Liu, C. Yu, H. Ji, J. Zuo, J. Zhao and L. Zang, *J. Am. Chem. Soc.*, 2010, **132**, 5743.
4 S. Ji, H. Wang, T. Wang and D. Yan, *Adv. Mater.*, 2013, **25**, 1755.
5 J. T Kirner, J. J Stracke, B. A Gregg and R. G Finke, *ACS Appl. Mater. Interfaces*, 2014, **6**, 13367.
6 T. Van der Boom, R. T. Hayes, Y. Zhao, P. J. Bushard, E. A. Weiss and M. R. Wasielewski, *J. Am. Chem. Soc.*, 2002, **124**, 9582.
7 X. Li, L. E. Sinks, B. Rybtchinski and M. R. Wasielewski, *J. Am. Chem. Soc.*, 2004, **126**, 10810.
8 J. Feng, B. Liang, D. Wang, H. Wu, L. Xue and X. Li, *Langmuir*, 2008, **24**, 11209.
9 J. Zhou, L. Xue, Y. Shi, X. Li, Q. Xue and S. Wang, *Langmuir*, 2012, **28**, 14386.
10 L. Zang, Y. Che and Y. S. Moore, *Acc. Chem. Res.*, 2008, **41**, 1596.
11 C. Xue, O. Birel, M. Gao, S. Zhang, L. Dai, A. Urbas and Q. Li, *J. Phys. Chem. C*, 2012, **116**, 10396.
12 Y. Huang, B. Quan, Z. Wei, G. Liu and L. Sun, *J. Phys. Chem. C*, 2009, **113**, 3929.
13 A. L. Briseno, S. C. B. Mannsfeld, C. Reese, J. M. Hancock, Y. Xiong, S. A. Jenekhe, Z. Bao and Y. Xia, *Nano Lett.*, 2007, **7**, 2847.
14 K. Balakrishnan, A. Datar, T. Naddo, J. Huang, R. Oitker, M. Yen, J. Zhao and L. Zang, *J. Am. Chem. Soc.*, 2006, **128**, 7390.
15 D. Ke, C. Zhan, S. Xu, X. Ding, A. Peng, J. Sun, S. He, A. D. Q. Li and J. Yao, *J. Am. Chem. Soc.*, 2011, **133**, 11022.
16 L. Zhu, W. Wu, M. Zhu, J. J. Han, J. K. Hurst and A. D. Q. Li, *J. Am. Chem. Soc.*, 2007, **129**, 3524.
17 F. J. M. Hoeben, P. Jonkheijm, E. W. Meijer and A. P. H. J. Schenning, *Chem. Rev.*, 2005, **105**, 1491.
18 Y. Chen, Y. Feng, J. Gao and M. Bouvet, *J. Colloid Interface Sci.*, 2012, **368**, 387.
19 S. Xu, J. Sun, D. Ke, G. Song, W. Zhang and C. Zhan, *J. Colloid Interface Sci.*, 2010, **349**, 142.
20 X. Yang, X. Xu and H. Ji, *J. Phys. Chem. B*, 2008, **112**, 7196.
21 X. Zhang, Z. Chen and F. Würthner, *J. Am. Chem. Soc.*, 2007, **129**, 4886.

22 Y. Li, X. Li, Y. Li, H. Liu, S. Wang, H. Gan, J. Li, N. Wang, X. He and D. Zhu, *Angew. Chem., Int. Ed.*, 2006, **45**, 3639.
23 C. Huang, L. Wen, H. Liu, Y. Li, X. Liu, M. Yuan, J. Zhai, L. Jiang and D. Zhu, *Adv. Mater.*, 2009, **21**, 1721.
24 Y. Wang, Y. Chen, R. Li, S. Wang, W. Su, P. Ma, M. R. Wasielewski, X. Li and J. Jiang, *Langmuir*, 2007, **23**, 5836.
25 Y. Chen, Y. Kong, Y. Wang, P. Ma, M. Bao and X. Li, *J. Colloid Interface Sci.*, 2009, **330**, 421.
26 C. Thalacker and F. Würthner, *Adv. Funct. Mater.*, 2002, **12**, 209.
27 L. Xue, H. Wu, Y. Shi, H. Liu, Y. Chen and X. Li, *Soft Matter*, 2011, **7**, 6213.
28 F. Würthner, C. Thalacker, S. Diele and C. Tschierske, *Chem. – Eur. J.*, 2001, **7**, 2245.
29 Z. Chen, U. Baumeister, C. Tschiersk and F. Würthner, *Chem. – Eur. J.*, 2007, **13**, 450.
30 Y. Chen, L. Chen, G. Qi, H. Wu, Y. Zhang and L. Xue, *Langmuir*, 2010, **26**, 12473.
31 J. Hu, W. Kuang, K. Deng, W. Zou, Y. Huang, Z. Wei and C. F. J. Faul, *Adv. Funct. Mater.*, 2012, **22**, 4149.
32 Y. Chen, M. Bouvet, T. Sizun, Y. Gao, C. Plassard, E. Lesniewskac and J. Jiang, *Phys. Chem. Chem. Phys.*, 2010, **12**, 12851.
33 E. W. Huge, *J. Am. Chem. Soc.*, 1941, **63**, 1737.
34 C. Hippius, I. H. M. Van Stokkum, E. Zangrando, R. M. Williams, M. Wykes, D. Beljonne and F. Würthner, *J. Phys. Chem. C*, 2008, **112**, 14626.
35 X. Zhang, D. Gao, J. Gao, P. Zhu, M. Bouvet and Y. Chen, *RSC Adv.*, 2014, **4**, 14807.
36 P. Ma, Y. Chen, Y. Bian and J. Jiang, *Langmuir*, 2010, **26**, 3678.
37 Y. Che, A. Datar, X. Yang, T. Naddo, J. Zhao and L. Zang, *J. Am. Chem. Soc.*, 2007, **129**, 6354.
38 J. Feng, Y. Zhang, C. Zhao, R. Li, W. Xu, X. Li and J. Jiang, *Chem. – Eur. J.*, 2008, **14**, 7000.

